PET and SPECT for Detection of Tumor Progression in Irradiated Low-Grade Astrocytoma: A Receiver-Operating-Characteristic Analysis

Marcus Henze, MD[1,2]; Ashour Mohammed, PhD[1]; Heinz P. Schlemmer, MD[3]; Klaus K. Herfarth, MD[4]; Simone Hoffner, MD[1,2]; Sabine Haufe, MD[1]; Walter Mier, PhD[1]; Michael Eisenhut, PhD[5]; Jürgen Debus, MD, PhD[4]; and Uwe Haberkorn, MD[1,2]

[1]Department of Nuclear Medicine, University of Heidelberg, Heidelberg, Germany; [2]Clinical Cooperation Unit Nuclear Medicine, German Cancer Research Center, Heidelberg, Germany; [3]Department of Diagnostic Radiology, Eberhard-Karls University, Tübingen, Germany; [4]Department of Radiation Oncology, University of Heidelberg, Heidelberg, Germany; and [5]Division of Radiochemistry and Radiopharmacology, German Cancer Research Center, Heidelberg, Germany

Differentiation between tumor progression and radiation necrosis is one of the most difficult tasks in oncologic neuroradiology. Functional imaging of tumor metabolism can help with this task, but the choice of tracer is still controversial. This prospective study following up irradiated low-grade astrocytoma (LGA) was, to our knowledge, the first receiver-operating-characteristic (ROC) analysis that intraindividually evaluated the diagnostic performance of the SPECT tracers 3-[^{123}I]iodo-α-methyl-L-tyrosine (IMT) and ^{99m}Tc(I)-hexakis(2-methoxyisobutylisonitrile) (MIBI) and the PET tracer ^{18}F-FDG. **Methods:** We examined 17 patients, initially with histologically proven LGA and treated by stereotactic radiotherapy, who presented with new gadolinium-diethylenetriaminepentaacetic acid–enhancing lesions ($n = 26$) on MRI. At that time, MRI could not differentiate between progressive tumor and nonprogressive tumor. This MRI examination was closely followed by ^{18}F-FDG PET and by ^{99m}Tc-MIBI and ^{123}I-IMT SPECT. Lesions were classified as progressive tumor ($n = 17$) or nonprogressive tumor ($n = 9$) on the basis of prospective follow-up (through clinical examination, MRI, and proton MR spectroscopy) for 26.6 ± 6.6 mo after PET or SPECT. **Results:** ^{123}I-IMT yielded the best ROC characteristics and was the most accurate for classification, with an area under the ROC curve (A_z) of 0.991. The A_z of ^{18}F-FDG (0.947) was not significantly lower than that of ^{123}I-IMT. The difference in the A_z of ^{99m}Tc-MIBI (0.713) from the A_z of the other tracers used in our study was highly significant ($P \leq 0.01$). ^{99m}Tc-MIBI SPECT was of low accuracy and, especially, of poor sensitivity even at modest specificity values. **Conclusion:** ^{123}I-IMT SPECT imaging of amino acid transport accurately detects tumor progression in patients with irradiated LGA. In contrast to ^{123}I-IMT, ^{18}F-FDG PET was slightly less accurate for classification, and ^{99m}Tc-MIBI SPECT was of limited value. Imaging of amino acid transport with ^{123}I-IMT is a valuable additional tool for the follow-up of LGA, allowing early, noninvasive differentiation of lesions with ambiguous morphology after irradiation.

Key Words: ^{18}F-FDG; 3-^{123}I-iodo-α-methyl-L-tyrosine; ^{99m}Tc(I)-hexakis(2-methoxyisobutylisonitrile); radiotherapy; astrocytoma

J Nucl Med 2004; 45:579–586

The American Cancer Society estimates that 16,800 new intracranial tumors are diagnosed in the United States each year. In persons older than 20 y, gliomas compose more than 90% of primary intracranial tumors. About 25% of gliomas are low-grade astrocytomas (LGAs). Most LGAs are not amenable to complete resection, and radiotherapy is the most effective nonsurgical therapy (*1*).

Many low-grade gliomas convert to high-grade gliomas during follow-up. Anatomic distortion and scarring after therapy often impair detection of residual or recurrent disease. Differentiation between tumor recurrence or progression and radiation injury or necrosis is one of the most difficult tasks in oncologic neuroradiology. In addition to clinical findings, contrast-enhanced MRI is used to measure therapy response. Single conventional MRI scans often fail to distinguish recurrent tumor from radiation injury or necrosis, because both cause disturbances of the blood–brain barrier (BBB) leading to nonspecific contrast-medium enhancement. Even biopsy of an edematous or gliotic site is often nondiagnostic.

Functional imaging of tumor metabolism can help overcome this issue. For detection of glioma recurrence, a variety of tracers have been used. Some authors reported that glucose metabolism measured by ^{18}F-FDG PET could differentiate radiation necrosis from recurrent tumor (*2*), whereas other groups questioned its value (*3*). Furthermore, SPECT with 3-^{123}I-iodo-α-methyl-L-tyrosine (IMT) for im-

Received Jul. 8, 2003; revision accepted Dec. 8, 2003.

For correspondence or reprints contact: Marcus Henze, MD, Department of Nuclear Medicine, University of Heidelberg, Im Neuenheimer Feld 400, 69120 Heidelberg, Germany.

E-mail: marcus.henze@med.uni-heidelberg.de

aging amino acid transport and with the tumor-affine tracer ^{99m}Tc(I)-hexakis(2-methoxyisobutylisonitrile) (MIBI) is used frequently, although the value of ^{99m}Tc-MIBI has been questioned (*4*). Few studies have dealt with previously irradiated brain tumors, and those tumors have been mostly of higher grade. Still strongly controversial is the question of which tracer gives more accurate information on tumor progression or recurrence. Therefore, studies directly comparing the diagnostic utility of different tracers for this clinically highly complex and important task have been recommended (*5*). In a recently published study, we compared the SPECT tracers ^{123}I-IMT and ^{99m}Tc-MIBI (*6*) for sensitivity and specificity. The present prospective study on the follow-up of irradiated LGAs was, to our knowledge, the first receiver-operating-characteristic (ROC) analysis that intraindividually evaluated the diagnostic performance of SPECT tracers (^{123}I-IMT and ^{99m}Tc-MIBI) and PET tracers (^{18}F-FDG).

MATERIALS AND METHODS

Patients

We included 17 patients (11 male, 6 female; mean age, 44.5 ± 10.6 y) who initially had biopsy-proven LGAs according to the criteria of the World Health Organization (*7*). The study was approved by the local ethical committee, and all patients gave informed consent before being included in the study. The patients fasted overnight before administration of tracers. Tracers were injected in a room with dimmed light, no conversation, and low ambient noise coming primarily from the scanner gantry fans. The patients closed their eyes, but their ears were left unplugged to avoid the frontal activation that occurs during total sensory deprivation. Treatment was by stereotactic radiotherapy (59.0 ± 4.4 Gy). On average, 35.3 ± 21.0 mo after radiotherapy, the patients presented with new gadolinium-diethylenetriaminepentaacetic acid (DTPA)–enhancing lesions (n = 26) on MRI, which, at that time, could not differentiate between progressive tumor (PT) and non-PT (nPT). Tumor invasiveness and heterogeneity can lead to the appearance of multiple separate gadolinium-DTPA–enhancing lesions during the course of the disease. Multifocal lesions can appear as separate distinct masses, because different grades of tumor, with variable regions of BBB disruption and gadolinium-DTPA enhancement, may exist within the same tumor. The MRI examination was closely followed by PET or SPECT. Lesions were classified as PT or nPT on the basis of prospective follow-up (through clinical examination, MRI, and proton MR spectroscopy) for 26.6 ± 6.6 mo after PET or SPECT. The 17 patients were studied as part of a larger group of consecutive LGA patients in whom gadolinium-DTPA–enhancing lesions had developed during follow-up. The inclusion criterion was the feasibility of a clear-cut classification into PT or nPT during follow-up after PET or SPECT. In the PT group (17 lesions), patients received 59.3 ± 3.9 Gy. The interval between radiotherapy and PET or SPECT was 39.1 ± 21.4 mo. Lesions were followed up for an additional 24.6 ± 5.6 mo after PET or SPECT until the final classification was made. The patients in the nPT group (9 lesions) received 58.5 ± 5.3 Gy. In this group, the interval between radiotherapy and PET or SPECT was 27.7 ± 18.9 mo and the follow-up after PET or SPECT was 30.3 ± 6.9 mo. The classification was not influenced by the results of PET or SPECT. MRI, including multiplanar T1-weighted and T2-weighted spin-echo imaging followed by multiplanar gadolinium-DTPA–enhanced T1-weighted imaging, was repeated every 3–6 mo using a 1.5-T MRI scanner (Siemens AG). Intervals were shortened if symptoms worsened. A lesion was classified as PT if the T2-weighted hyperintense area increased by more than 25% or if the gadolinium-DTPA–enhancing area enlarged. Repeated proton MR spectroscopy, because shown to improve differentiation between treatment-induced necrosis and residual or recurrent brain tumor, was included in the MRI protocol in ambiguous cases (*8*). The combined MRI/^{1}H-MR spectroscopy examination included multiplanar T1-weighted and T2-weighted spin-echo imaging and single-voxel ^{1}H-MR spectroscopy (point-resolved spectroscopy; repetition time = 1,500 ms, echo time = 135 ms) of lesions, followed by multiplanar gadolinium-DTPA–enhanced T1-weighted MRI. The horizontal or frequency axes were normalized to a strong signal of known origin, and the locations of the peaks were given as parts per million relative to the known signal. The relative signal intensity ratios for choline (3.20 ppm, membrane phospholipid turnover), creatine (3.93 and 3.04 ppm, cellular energy metabolism), and *N*-acetylaspartate (2.02 ppm, neuronal integrity) were calculated.

^{99m}Tc-MIBI SPECT

Preparation and quality control of ^{99m}Tc-MIBI (sestamibi; DuPont Pharma S.A.) were according to the manufacturer's instructions. In 16 patients, SPECT was started 15 min after intravenous injection of 695 ± 65 MBq of ^{99m}Tc-MIBI. SPECT was performed using a dual-head γ-camera (MULTISPECT2; Siemens) equipped with high-resolution collimators. Sixty-four projections were obtained over 360°. Data were registered for 40 s in each projection and were recorded in a 64 × 64 matrix. Images were reconstructed by filtered backprojection using a Butterworth filter (frequency cutoff = 0.5 Nyquist; order = 8). Attenuation correction (first-order, 0.12/cm) was performed using the postreconstruction method of Chang (*9*).

^{123}I-IMT SPECT

To prevent possible uptake of free iodine, the thyroid gland was blocked with sodium perchlorate. ^{123}I-IMT was prepared using essentially the KIO_3/^{123}I-iodide method described previously (*10*). ^{123}I-IMT accumulates in brain and tumor tissue, reaching a maximum after 15 min, with a washout of 20%–45% at 60 min after injection (*11*). Therefore, in all 17 patients, imaging began 10 min after intravenous injection of 285 ± 59 MBq ^{123}I-IMT. The γ-camera system (MULTISPECT 2) was the same as for the sestamibi examination, but equipped with medium-energy collimators, as recommended for ^{123}I (*12*). Sixty-four projections (40 s each) were acquired over 360° using a 64 × 64 matrix. Images were reconstructed by filtered backprojection using a Butterworth filter (frequency cutoff = 0.5 Nyquist, order = 8). First-order attenuation correction (0.12/cm) was performed, using Chang's method (*9*).

^{18}F-FDG PET

In all 17 patients, 209 ± 40 MBq of ^{18}F-FDG were injected. Starting 45 min after injection, a 20-min emission scan was acquired, followed by a 5-min transmission scan using 3 ^{68}Ge line sources. Measurements were obtained with a whole-body PET system (ECAT EXACT HR^{+}; CTI) covering 155 mm in the axial field of view (63 transversal slices; thickness of each slice, 2.4 mm). The scanner consisted of 4 rings, each having 72 bismuth germanate detector blocks. Data were acquired in the more sensitive 3-dimensional mode without interslice tungsten septa. Quan-

tification in 3-dimensional mode was found to be equivalent to that in the 2-dimensional mode for radioactivities used clinically (*13*). The matrix size was 128 × 128 pixels. Iterative image reconstruction used the ordered-subsets expectation maximization algorithm.

Data Analysis

The images were analyzed by calculating lesion-to-normal ratios (l/n). Areas of abnormal tracer uptake were defined as focally increased uptake or as asymmetric uptake, compared with the contralateral side. Uptake ratios were calculated using reference regions in the contralateral hemisphere, because of the limitations of SPECT in providing absolute quantification. Regions of interest (ROIs) were delineated on the 2 transaxial slices with the highest tracer uptake in the lesion. The scanner software was used to place ROIs over the lesions, to include all pixels having at least 70% of the maximum uptake of the lesion. For this purpose, the cursor was manually positioned at the border of the lesion. A circular contour was generated automatically, starting and ending at this point and including the same percentage as the maximum pixel value in this area. Then, the percentage was adjusted to 70% of the maximum pixel value in this area. Afterward, a mean was calculated from this particular set of pixels. Some gadolinium-DTPA–enhancing lesions showed no elevated uptake of ^{123}I-IMT, ^{99m}Tc-MIBI, or ^{18}F-FDG. In these patients, ROIs were placed in accord with the MRI reference. Because a 70% threshold could not be determined, ROIs were defined manually in these cases. For that purpose, MRI scans were visually inspected and ROIs were manually delineated on PET and SPECT scans, enclosing the gadolinium-DTPA–enhancing lesion on MRI. Afterward, a mean was calculated from this particular set of pixels. ^{123}I-IMT and ^{99m}Tc-MIBI uptake was measured semiquantitatively by calculating l/n ratios for all gadolinium-DTPA–enhancing lesions. As a reference region, the lesion ROI was mirrored to the contralateral hemisphere. Software automatically performed the mirroring procedure, which approximated the interhemispheric fissure. In all patients, the position of the contralateral ROI was manually adjusted to fit the exact position of the lesion ROI. In cases of anatomic distortion secondary to mass effects or edema, visually inspected MRI scans were considered.

The calculation of ratios based on uninvolved contralateral structures was recommended for analysis of ^{18}F-FDG PET studies of the brain (*14*). Although the possibility cannot be excluded that the contralateral hemisphere might exhibit reduced metabolism because of interruption of association fibers between hemispheres, this effect has been shown to be negligible (*15*). For ^{18}F-FDG, semiquantitative l/n ratios based on a separate ROI determining the mean uptake of the uninvolved contralateral gray matter (70% isocontour), as a reference, were calculated (*14,16*).

For conventional statistical analysis, SigmaStat software (version 2.0; Jandel Corp.) was used. The Mann–Whitney rank sum test was used to compare the PT and nPT groups.

The choice of cutoff values is arbitrary, and one can obtain different results by selecting different values. A general solution to the arbitrary-thresholds problem is the ROC curve. One selects many cutoff points, calculates the sensitivity and specificity for each cutoff value, and plots sensitivity against 1 − specificity. Such a curve describes the compromises that can be made between sensitivity and specificity and is helpful to determine a clinically adequate cutoff. Another advantage of this method is that the area under the ROC curve (A_z) tends to be robust, even when the normality assumption is violated. The shapes of the underlying populations do not significantly affect A_z. Relative to traditional methods, ROC methods better estimate predictive power because of their independence from cutoff values and their attention to the impact of prevalence on optimal cutoff values.

The diagnostic accuracy of ^{123}I-IMT, ^{99m}Tc-MIBI, and ^{18}F-FDG was analyzed using the ROCKIT 0.9B software package for Windows (Microsoft) developed by Charles E. Metz (University of Chicago). The A_z and its SE (SE [A_z]) were calculated as a measure of the likelihood of a correct test decision using a global decision variable (*17*). This measure represents the predicted diagnostic accuracy of the diagnostic tests and is independent of disease prevalence and decision-making threshold. Another goal was to find optimized l/n decision thresholds for adequate tradeoffs between sensitivity and specificity. A_z was calculated parametrically with a bivariate binormal model. The ROCKIT software categorizes continuously distributed input data to produce a spread of operating points on each ROC curve. The datasets are then analyzed to obtain maximum-likelihood estimates of the conventional binormal intercept, slope, and category-boundary parameters. Differences in the areas under the ROC curves (A_z) were tested for significance using a bivariate χ^2 test of the simultaneous differences between the "a" and "b" parameters describing the 2 ROC curves (null hypothesis: the datasets arose from the same binormal ROC curve). A true-positive fraction (TPF) test was conducted at false-positive fraction (FPF) = 0.05, FPF = 0.1, and FPF = 0.2 (i.e., specificities of 95%, 90%, and 80%, respectively) to compare the sensitivity of the tracers at low FPFs. FPF was defined as 1 – specificity. Sensitivity (synonym for TPF) was defined as number of true positives/(number of true positives + number of false negatives), and specificity was defined as number of true negatives/(number of true negatives + number of false positives). The TPF test is a univariate *z* score test of the difference between the TPFs on the 2 ROC curves at a selected FPF (null hypothesis: the datasets arose from the same binormal ROC curve, having the same TPF at the selected FPF).

For all tests, the 0.05 level was considered statistically significant. Because 3 tracers were used, the Bonferroni-corrected *P* value was 0.05/3 = 0.017.

RESULTS

^{99m}Tc-MIBI SPECT

In the nPT group, l/n ratios varied from 1.0 to 7.0, with a mean (±SD) of 1.8 ± 1.8. L/n ratios in the PT group ranged from 1.0 to 8.6, with a mean of 3.7 ± 2.8. For the whole population of patients, the mean l/n ratio was 3.0 ± 2.6. PT and nPT did not significantly differ ($P = 0.206$) (Fig. 1). Using ^{99m}Tc-MIBI, the A_z (±SE) was 0.713 ± 0.170 (Fig. 2; Table 1). Differences in A_z between examined tracers were tested for significance using a χ^2 test as well as *t* tests conducted at different FPFs ranging from 0.05 to 0.2. When ^{99m}Tc-MIBI was compared with both ^{123}I-IMT and ^{18}F-FDG, differences were highly significant (Table 2). A merely acceptable trade-off between sensitivity and specificity for separating PT from nPT was found at l/n thresholds of 1.3–1.5. At these decision thresholds, FPF ranged from 0.23 to 0.25 and TPF ranged from 0.54 to 0.55 (Table 3).

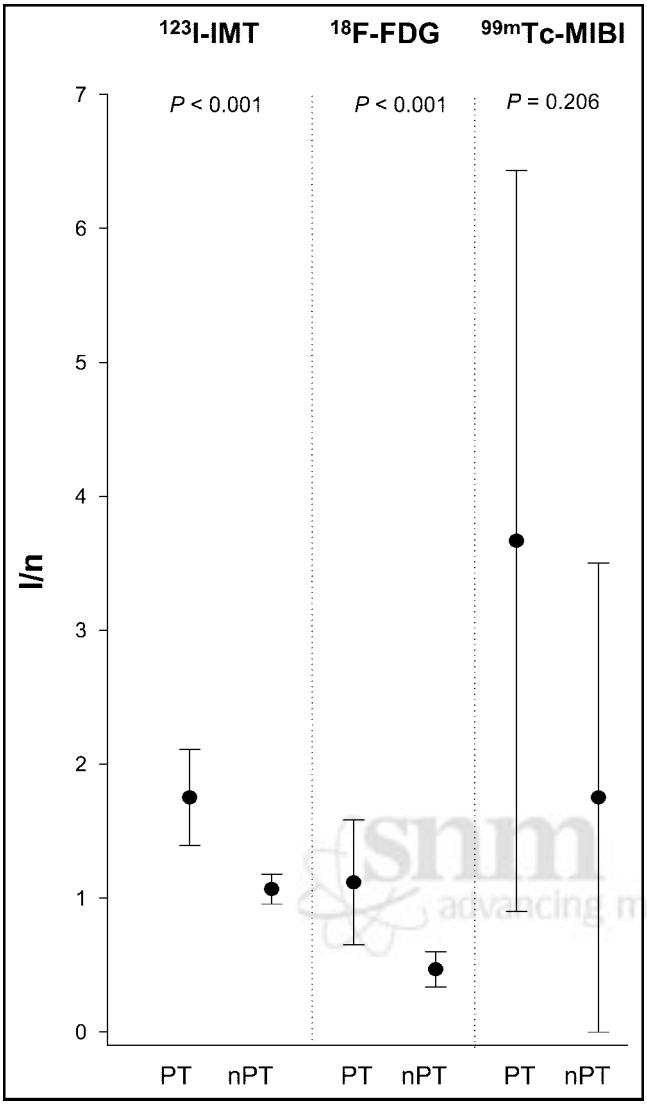

FIGURE 1. L/n ratios (mean ± SD) for ^{123}I-IMT, ^{18}F-FDG, and ^{99m}Tc-MIBI. In contrast to ^{99m}Tc-MIBI, both ^{123}I-IMT and ^{18}F-FDG allow highly significant differentiation between PT and nPT groups.

^{123}I-IMT SPECT

L/n ratios in the PT group ranged from 1.2 to 2.8, with a mean of 1.7 ± 0.3 (Fig. 1). The l/n ratios in the nPT group varied from 1.0 to 1.3, with a mean of 1.1 ± 0.1. Significantly higher ratios were found in PT than in nPT ($P < 0.001$) (Fig. 1). A_z as a measure of the likelihood of a correct test decision with a global decision variable was 0.991 ± 0.014 for ^{123}I-IMT (Fig. 2; Table 1). Testing for significance of differences in A_z using χ^2 and FPF tests revealed highly significant differences between ^{123}I-IMT and ^{99m}Tc-MIBI. In contrast, A_z did not significantly differ between ^{123}I-IMT and ^{18}F-FDG (Table 2). ^{123}I-IMT demonstrated a good trade-off between sensitivity and specificity at l/n thresholds between 1.27 and 1.35. For these decision thresholds, FPF ranged from 0.02 to 0.05 and TPF ranged from 0.94 to 0.96 (Table 4). There was only a moderate correlation between l/n ratios of ^{123}I-IMT and ^{18}F-FDG ($r = 0.64$) and only a weak correlation between ^{123}I-IMT and ^{99m}Tc-MIBI ($r = 0.53$).

^{18}F-FDG PET

In the PT group, l/n ratios ranged from 0.2 to 2.0, with a mean of 1.1 ± 0.5. The l/n ratios in the nPT group varied from 0.4 to 0.7, with a mean of 0.5 ± 0.1 (Fig. 1). Using ^{18}F-FDG, significantly higher l/n ratios were found in the PT group than in the nPT group ($P < 0.001$) (Fig. 1). The A_z was 0.947 ± 0.052 for ^{18}F-FDG (Fig. 2; Table 1). χ^2 and FPF tests for evaluation of A_z revealed highly significant differences between ^{18}F-FDG and ^{99m}Tc-MIBI. In contrast, A_z was not significantly different between ^{18}F-FDG and ^{123}I-IMT (Table 2). Using l/n thresholds between 0.6 and 0.8, ^{18}F-FDG demonstrated a good trade-off between sensitivity and specificity. For these decision thresholds, FPF ranged from 0.02 to 0.05, whereas TPF ranged from 0.83 to 0.86 (Table 5).

DISCUSSION

Although a comparison of different tracers for this clinically relevant task has been proposed (*5*), no study applying ^{18}F-FDG, ^{123}I-IMT, and ^{99m}Tc-MIBI in the same population has, to our knowledge, been published. Furthermore, the studies using one of these tracers included only small numbers of irradiated low-grade tumors. We investigated the classification accuracy of these tracers using ROC analysis. A_z represents the predicted diagnostic accuracy of the diagnostic tests and, unlike sensitivity and specificity, is independent of disease prevalence and decision-making threshold. Because the shape of the ROC curves for different tracers can vary, even with the same A_z parameter, the sensitivity at low FPFs (i.e., high specificity) was also investigated. As in most other studies, the classification of our patients relied on clinical follow-up and not on biopsy. Particularly after irradiation, gliomas are not homogeneous. Even stereotactically guided biopsy is often inaccurate, because samples may be taken from scarred or gliotic areas and not necessarily represent total tumor viability (*18*). Furthermore, the presence of morphologically intact tumor cells did not indicate recurrence or progression, because these cells may be unable to proliferate after therapy. In our series of patients, lesions were classified on the basis of prospective clinical follow-up, including serial MRI and proton MR spectroscopy for an average of 26.6 mo after PET or SPECT for a suggestive new cerebral lesion, and 61.9 mo after completion of radiotherapy. Also, survival of patients with low-grade gliomas is prolonged, and long follow-up times are necessary. We believe that a mean prospective follow-up of 26.6 mo after the appearance of new areas of contrast enhancement (suggestive of anaplastic tumor areas) on MRI is sufficient to distinguish real progress from a radiation-induced disturbance of the BBB. Progressive disease was confirmed by repeated MRI, which showed further enlargement of the contrast-enhanced areas,

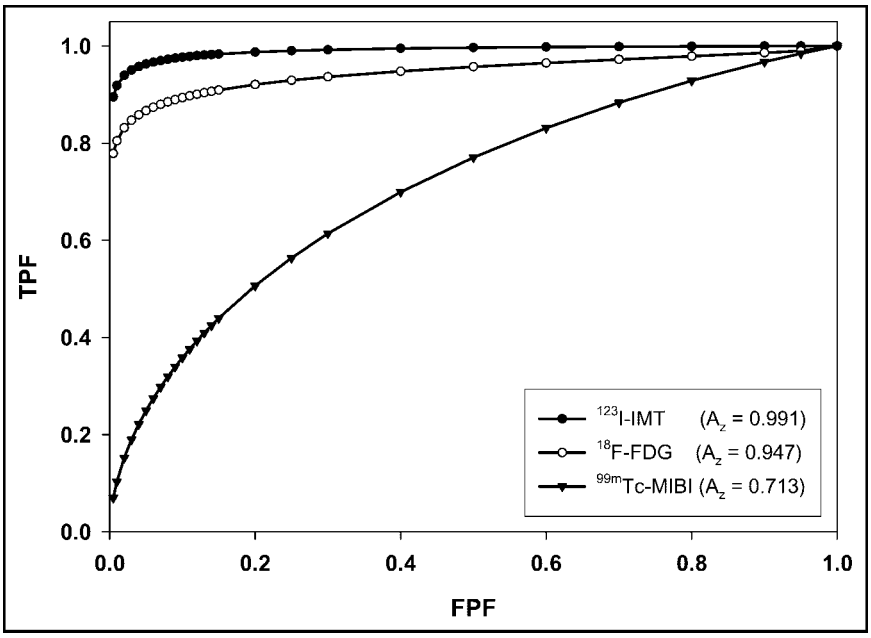

FIGURE 2. ROC curves for ^{123}I-IMT, ^{18}F-FDG, and ^{99m}Tc-MIBI.

and by MRI spectroscopy examinations. MRI was repeated every 3–6 mo. Intervals were shortened if symptoms worsened or MRI showed progression. The suspected higher-grade anaplastic tumor parts are much more aggressive than genuine low-grade gliomas. Karim et al. reported a progression-free median survival of approximately 5.5 y after radiotherapy of low-grade gliomas. However, in progressive disease, the median overall survival was only 24 mo (*19*). In addition, our follow-up period is one of the longest reported and is more than 4-fold longer than those of comparable studies (*20–22*).

The difference between the A_z of ^{99m}Tc-MIBI (0.713) and the A_z of the other tracers used in our study was highly significant (Table 2). ^{99m}Tc-MIBI SPECT examinations resulted in low accuracy and, especially, in poor sensitivity even at modest specificity values. The results of the more elaborate ROC analysis using variable cutoff values agreed with our previous results comparing ^{99m}Tc-MIBI and ^{123}I-IMT at a fixed cutoff value (l/n = 1.3), resulting in a distinctly higher sensitivity and specificity for ^{123}I-IMT (*6*). In contrast to ^{18}F-FDG and ^{123}I-IMT, ^{99m}Tc-MIBI did not allow exclusion of PT, because of its high rate of false-negative results. Uptake of ^{99m}Tc-MIBI is determined by multiple factors, such as vascular supply; disruption of the BBB; density, viability, and oxygenation of tumor cells; and mitochondrial membrane potential (*23*). Furthermore, in delayed imaging (2–4 h after injection), uptake is related to the expression of the multidrug resistance pump P-glycoprotein (*24*). When ^{99m}Tc-MIBI was applied to pretreated high-grade gliomas, promising results were reported (*21*), whereas studies examining miscellaneous tumor grades showed sensitivities of 73%–88% for detecting tumor relapse. Specificity was 85%–91%, PPV was 91%–98%, and NPV was 60%–63%, respectively (*20,22*). However, the study reporting the highest values included only a small percentage (27%) of low-grade tumors (*20*). In contrast, the lowest sensitivities and specificities were observed in the study with the highest percentage (50%) of low-grade gliomas (*22*). In 6 previously irradiated gliomas, solely of low grade, ^{99m}Tc-MIBI could not differentiate between tumor and radiation necrosis (*25*). Staudenherz et al. recently questioned the value of ^{99m}Tc-MIBI for the detection of high-grade recurrences after chemotherapy and suggested that retention of ^{99m}Tc-MIBI reflects simply damage of the BBB (*4*). Within 5 y after initial diagnosis, at least 50% of

TABLE 1
A_z, SE (A_z), and Parameters "a" (Ordinate Intercept) and "b" (Slope) Describing the ROC curves for ^{18}F-FDG, ^{123}I-IMT, and ^{99m}Tc-MIBI

Parameter	^{18}F-FDG PET	^{123}I-IMT SPECT	^{99m}Tc-MIBI SPECT
A_z	0.947	0.991	0.713
SE (A_z)	0.052	0.014	0.170
a	1.720	2.712	0.741
b	0.370	0.569	0.861

TABLE 2
P Values for Differences in ROC Curves, Tested for Significance Using the Bivariate χ^2 Test and the TPF test at Different FPFs

		TPF test		
Comparison	χ^2 test	FPF = 0.2	FPF = 0.1	FPF = 0.05
^{18}F-FDG vs. ^{123}I-IMT	0.5330	0.1318	0.1466	0.2154
^{18}F-FDG vs. ^{99m}Tc-MIBI	0.0032	0.0005	0.0004	0.0009
^{123}I-IMT vs. ^{99m}Tc-MIBI	0.0112	0.0074	0.0014	0.0023

TABLE 3
Decision Thresholds (l/n) for ^{99m}Tc-MIBI

l/n	FPF	TPF
3.2	0.189	0.493
1.5	0.229	0.541
1.3	0.250	0.550

TABLE 5
Decision Thresholds (l/n) for ^{18}F-FDG

l/n	FPF	TPF
0.8	0.021	0.833
0.6	0.045	0.862
0.3	0.158	0.911

LGAs undergo malignant transformation and a BBB disruption develops (*26*). However, BBB disruption also occurs in radiation necrosis. Accordingly, gadolinium-DTPA enhancement on MRI indicated damage of the BBB in all our patients, as a prerequisite for ^{99m}Tc-MIBI uptake. In accordance with previous reports, we also found the detectability of paraventricular lesions to be limited (*27*). The explanation was the high physiologic ^{99m}Tc-MIBI uptake in the choroid plexus. The low tumor-detection rate of ^{99m}Tc-MIBI, compared with that of ^{123}I-IMT, could not be explained by technical issues, because the same camera system and acquisition parameters were used for both SPECT tracers.

^{123}I-IMT yielded the best ROC characteristics and the highest classification accuracy, with an A_z of 0.991. For decision thresholds (l/n) between 1.25 and 1.35, ^{123}I-IMT offered a good trade-off between sensitivity (>94%) and specificity (>93%). Choosing an l/n threshold of 1.35, associated with a high specificity of 98%, resulted in only a slight reduction of sensitivity—to 94%. A_z was significantly higher for ^{123}I-IMT than for ^{99m}Tc-MIBI (A_z = 0.713) but not for ^{18}F-FDG (A_z = 0.947). Because competition of ^{123}I-IMT with structurally related naturally occurring L-amino acids for transport into brain and tumor could decrease sensitivity (*28*), we examined all patients while they were fasting. In contrast to ^{11}C-tyrosine, ^{123}I-IMT uptake reflects amino acid transport rather than the protein synthesis rate, because it is not incorporated into proteins. Both protein synthesis and amino acid transport are accelerated in high- and low-grade tumor tissue. The L-carrier system for large neutral amino acids mediates transport across the intact BBB (*28*). Because ^{123}I-IMT is not metabolized, it is washed out of the brain after reaching a maximum uptake at 15 min after injection (*11*,*29*). Excepting a few extracerebral applications, such as carcinomas of the hypopharynx or larynx (*30*), ^{123}I-IMT has been used mostly for brain tumors. It was shown to be promising for evaluating biologic activity and delineating intracerebral infiltration of gliomas (*11*,*16*,*31*). Most studies using ^{123}I-IMT during follow-up after treatment of brain tumors have included only a limited number ($n \leq 5$) of low-grade tumors (*32*,*33*). In one of the largest series, cerebral uptake of ^{123}I-IMT was determined in 27 patients, including 9 with low-grade tumors, of whom 3 underwent radiotherapy. In this study, the overall sensitivity for detecting recurrences was 78% and the specificity was 100% (*5*). Also, classification with ^{18}F-FDG was highly accurate. Its A_z (0.947) was somewhat (but not significantly) lower that that of ^{123}I-IMT, mainly because of the slightly lower sensitivity of ^{18}F-FDG (Fig. 2B). With ^{18}F-FDG PET, one might question whether gray matter or white matter should be used as a reference for semiquantitative analysis. For that reason, we additionally analyzed our PET data using white matter as a reference (data not shown). A close correlation was found between the l/n ratios based on gray-matter and white-matter reference regions (r = 0.95). A_z for gray matter (0.947) was slightly higher than A_z for white matter (0.921). A_z did not significantly differ between gray and white matter (P = 0.7). In the pretherapeutic setting, ^{18}F-FDG PET has proven useful in grading gliomas (*18*,*34*), assessing prognosis (*35*), and localizing the most aggressive areas before biopsy (*18*). In gliomas, ^{18}F-FDG uptake correlates with the grade of malignancy (*34*). For many years, ^{18}F-FDG PET has been regarded as the gold standard for noninvasive differentiation between radiation necrosis and recurrent high-grade gliomas, which exhibit increased glucose metabolism. For high-grade gliomas, the sensitivity ranges from 80% to 90%, whereas the specificity is between 50% and 90% (*36*). According to the literature, malignant progression is common in nearly two thirds of all recurrent LGAs. This finding is in accordance with the mean ^{18}F-FDG uptake in our PT group, slightly exceeding the mean uptake in cortical reference regions. Studying 13 patients with irradiated LGA, Roelcke et al. concluded that patients with tumors undergoing malignant progression during the course of the disease can be identified with ^{18}F-FDG PET (*37*). In contrast, other reports have indicated limitations because of the low l/n contrast. Ricci et al. reported a sensitivity of 73% and a specificity of only 56% for the detection of recurrences (*3*). The specificity of ^{18}F-FDG PET can be limited by an increased glycolysis in tissue reparation after surgery or radiotherapy and in inflammatory lesions (*38*). The sensitivity of ^{123}I-IMT SPECT (75%) for confirming low-grade recurrences (n = 8) proved to be superior to that of ^{18}F-FDG PET (50%), whereas specificity

TABLE 4
Decision Thresholds (l/n) for ^{123}I-IMT

l/n	FPF	TPF
1.35	0.023	0.943
1.27	0.050	0.960
1.15	0.231	0.989

could not be calculated in the study of Bader et al. (*39*). Sensitivity for detection of low-grade tumors, tumor progression, or tumor recurrence and clear definition of tumor extension can be reduced because of high glucose metabolism in surrounding normal brain tissue. Labeled amino acids may overcome this problem because of their low uptake in normal brain. As demonstrated with autoradiography, amino acids play a minor role in the metabolism of inflammatory cells, resulting in higher specificity for ^{123}I-IMT SPECT than for ^{18}F-FDG (*40*). Therefore, they were presumed to be more suitable for monitoring response to radio- or chemotherapy (*41*).

In prospect, the combination of the higher resolution of PET and a tracer that can image amino acid transport might be promising for further increasing the accuracy of classification, especially in small lesions. Recently, the synthesis of the ^{18}F-labeled amino acids ^{18}F-fluoro-ethyl-L-tyrosine and ^{18}F-fluoro-α-methyl-tyrosine was reported (*40*). Like ^{123}I-IMT SPECT, these tyrosine analogues reflect amino acid transport, and because of their ^{18}F label, they can benefit from the higher resolution of PET. Further clinical studies are required to determine their suitability for detecting tumor progression in irradiated LGA.

CONCLUSION

This multitracer ROC analysis of patients with irradiated LGA indicated that imaging of amino acid transport with ^{123}I-IMT SPECT had a high classification accuracy for detecting tumor progression. Despite its considerably higher spatial resolution in comparison with ^{123}I-IMT SPECT, the classification accuracy of ^{18}F-FDG PET was somewhat lower. The classification accuracy of both ^{123}I-IMT and ^{18}F-FDG was substantially higher than that of ^{99m}Tc-MIBI SPECT, which had limited value in the follow-up of these patients.

ACKNOWLEDGMENTS

The authors thank Stephanie Biedenstein, Heidi Adam, and Christian Schoppa for kind technical assistance with this study.

REFERENCES

1. Herfarth KK, Gutwein S, Debus J. Postoperative radiotherapy of astrocytomas. *Semin Surg Oncol.* 2001;20:13–23.
2. Ishikawa M, Kikuchi H, Miyatake S, et al. Glucose consumption in recurrent gliomas. *Neurosurgery.* 1993;33:28–33.
3. Ricci PE, Karis JP, Heiseman JE, et al. Differentiating recurrent tumor from radiation necrosis: time for re-evaluation of positron emission tomography? *AJNR.* 1998;19:407–413.
4. Staudenherz A, Fazeny B, Marosi C, et al. Does ^{99m}Tc-sestamibi in high-grade malignant brain tumors reflect blood-brain barrier damage only? *Neuroimage.* 2000;12:109–111.
5. Kuwert T, Woesler B, Morgenroth C, et al. Diagnosis of recurrent glioma with SPECT and iodine-123-alpha-methyl tyrosine. *J Nucl Med.* 1998;39:23–27.
6. Henze M, Mohammed A, Schlemmer H, et al. Detection of tumor progression in the follow-up of irradiated low grade gliomas: comparison of ^{123}I-alpha-methyl-L-tyrosine- and ^{99m}Tc-sestamibi SPECT. *Eur J Nucl Med.* 2002;29:1455–1461.
7. Kleinhues P, Burger PC, Scheithauer BW. Histological typing of tumors of the central nervous system (WHO). New York, NY: Springer; 1993.
8. Schlemmer HP, Bachert P, Herfarth KK, Zuna I, Debus J, van Kaick G. Proton MR spectroscopic evaluation of suspicious brain lesions after stereotactic radiotherapy. *AJNR.* 2001;22:1316–1324.
9. Chang LT. A method for attenuation correction in radionuclide computed tomography. *IEEE Trans Nucl Sci.* 1978;25:638–643.
10. Bubeck B, Eisenhut M, Heimke U, zum Winkel K. Melanoma affine radiopharmaceuticals. I. A comparative study of ^{131}I-labeled quinoline and tyrosine derivatives. *Eur J Nucl Med.* 1981;6:227–233.
11. Langen KJ, Ziemons K, Kiwit JC, et al. 3-[^{123}I]iodo-alpha-methyltyrosine and [methyl-^{11}C]-L-methionine uptake in cerebral gliomas: a comparative study using SPECT and PET. *J Nucl Med.* 1997;38:517–522.
12. Dobbeleir AA, Hambye AS, Franken PR. Influence of high-energy photons on the spectrum of iodine-123 with low- and medium-energy collimators: consequences for imaging with ^{123}I-labelled compounds in clinical practice. *Eur J Nucl Med.* 1999;26:655–658.
13. Brix G, Zaers J, Adam LE, et al. Performance evaluation of a whole-body PET scanner using the NEMA protocol. *J Nucl Med.* 1997;38:1614–1623.
14. Hustinx R, Smith RJ, Benard F, Bhatnagar A, Alavi A. Can the standardized uptake value characterize primary brain tumors on FDG-PET? *Eur J Nucl Med.* 1999;26:1501–1509.
15. Andrews RJ. Transhemispheric diaschisis: a review and comment. *Stroke.* 1991; 22:943–949.
16. Woesler B, Kuwert T, Morgenroth C, et al. Non-invasive grading of primary brain tumours: results of a comparative study between SPET with ^{123}I-alpha-methyl tyrosine and PET with ^{18}F-deoxyglucose. *Eur J Nucl Med.* 1997;24:428–434.
17. Metz CE, Herman BA, Shen JH. Maximum likelihood estimation of receiver operating characteristic (ROC) curves from continuously-distributed data. *Stat Med.* 1998;17:1033–1053.
18. Goldman S. Regional glucose metabolism and histopathology of gliomas: a study based on PET-guided stereotactic biopsy. *Cancer.* 1996;78:1098–1106.
19. Karim AMF, Maat B, Hatlevoll R, et al. A randomized trial on dose-response in radiation therapy of low-grade cerebral glioma: European Organization for Research and Treatment of Cancer (EORTC) study 22844. *Int J Radiat Oncol Biol Phys.* 1996;36:549–556.
20. Maffioli L, Gasparini M, Chiti A, et al. Clinical role of technetium-99m sestamibi single-photon emission tomography in evaluating pretreated patients with brain tumours. *Eur J Nucl Med.* 1996;23:308–311.
21. Soler C, Beauchesne P, Maatougui K, et al. Technetium-99m sestamibi brain single-photon emission tomography for detection of recurrent gliomas after radiation therapy. *Eur J Nucl Med.* 1998;25:1649–1657.
22. Lamy-Lhullier C, Dubois F, Blond S, et al. Importance of cerebral tomoscintigraphy using Tc-labeled sestamibi in the differential diagnosis of recurrent tumor vs. radiation necrosis in subtentorial glial tumors in the adult. *Neurochirurgie.* 1999;45:110–117.
23. Piwnica-Worms D, Kronauge JF, Chiu ML. Uptake and retention of hexakis (2-methoxy isobutyl isonitrile) technetium (I) in cultured chick myocardial cells: mitochondrial and plasma membrane potential dependence. *Circulation.* 1990; 82:1826–1838.
24. Leitha T, Glaser G, Lang S. Is early sestamibi imaging in head and neck cancer affected by MDR status, p53 expression or cell proliferation?. *Nucl Med Biol.* 1998;25:593–541.
25. Baillet G, Albuquerque L, Chen Q, Poisson M, Delattre JY. Evaluation of single-photon emission tomography imaging of supratentorial brain gliomas with technetium-99m-sestamibi. *Eur J Nucl Med.* 1994;21:1061–1066.
26. McCormack BM, Miller DC, Budzilovic GN, Voorhees GJ, Ransohoff J. Treatment and survival of low-grade astrocytoma in adults: 1977–1988. *Neurosurgery.* 1992;31:636–642.
27. Macapinlac A, Scott A, Caluser C, et al. Comparison of Tl-201 and Tc-99m MIBI with MRI in the evaluation of recurrent brain tumors [abstract]. *J Nucl Med.* 1992;33(suppl):867.
28. Langen KJ, Roosen N, Coenen H, et al. Brain and brain tumor uptake of L-3-[^{123}I]iodo-alpha-methyl tyrosine: competition with natural L-amino acids. *J Nucl Med.* 1991;32:1225–1228.
29. Langen KJ, Coenen HH, Roosen N, et al. SPECT studies of brain tumors with L-3-[^{123}I]iodo-alpha-methyl tyrosine: comparison with PET, ^{124}IMT and first clinical results. *J Nucl Med.* 1990;31:281–286.
30. Henze M, Mohammed A, Mier W, et al. Pretreatment evaluation of the hypopharynx and larynx carcinoma with ^{18}F-fluorodeoxyglucose, ^{123}I-alpha-methyl-tyrosine and ^{99m}Tc-hexakis-2-methoxyisobutylisonitrile. *Eur J Nucl Med.* 2002; 29:324–330.

31. Kuwert T, Morgenroth C, Woesler B, et al. Uptake of iodine-123-alpha-methyl tyrosine by gliomas and non-neoplastic brain lesions. *Eur J Nucl Med.* 1996;23: 1345–1353.
32. Guth-Tougelidis B, Müller S, Mehdorn MM, Knust EJ, Dutschka K, Reiners C. DL-3-^{123}I-iodo-alpha-methyltyrosine uptake in brain tumor recurrences. *Nuklearmedizin.* 1995;34:71–75.
33. Weber W, Bartenstein P, Gross MW, et al. Fluorine-18-FDG PET and iodine-123-IMT SPECT in the evaluation of brain tumors. *J Nucl Med.* 1997;38:802–808.
34. Delbeke D, Meyerowitz C, Lapidus RL, et al. Optimal cut-off levels of F-18-FDG uptake in the differentiation of low-grade from high-grade brain tumors with PET. *Radiology.* 1995;195:47–52.
35. De Witte O, Levivier M, Violon P, et al. Prognostic value positron emission tomography with [^{18}F]fluoro-2-deoxy-D-glucose in the low-grade glioma. *Neurosurgery.* 1996;39:470–476.
36. Langleben DD, Segall GM. PET in differentiation of recurrent brain tumor from radiation injury. *J Nucl Med.* 2000;41:1861–1867.
37. Roelcke U, Von Ammon K, Hausmann O, et al. Operated low grade astrocytomas: a long term PET study on the effect of radiotherapy. *J Neurol Neurosurg Psychiatry.* 1999;66:644–647.
38. Mochizuki T, Tsukamoto E, Kuge Y, et al. FDG uptake and glucose transporter subtype expressions in experimental tumor and inflammation models. *J Nucl Med.* 2001;42:1551–1555.
39. Bader JB, Samnick S, Moringale JR, et al. Evaluation of L-3-[^{123}I]iodo-alpha-methyltyrosine SPET and [^{18}F]fluorodeoxyglucose PET in the detection and grading of recurrences in patients pretreated for gliomas at follow-up: a comparative study with stereotactic biopsy. *Eur J Nucl Med.* 1999;26:144–151.
40. Kaim AH, Weber B, Kurrer MO, et al. ^{18}F-FDG and ^{18}F-FET uptake in experimental soft tissue infection. *Eur J Nucl Med.* 2002;29:648–654.
41. Otto L, Dannenberg P, Feyer P, et al. Iodine-123-methyl-tyrosine uptake of brain tumors: influence of radiotherapy [abstract]. *Eur J Nucl Med.* 1995;22(suppl): 796P.